Front. Chem. Eng. China 2008, 2(3): 269–275
DOI 10.1007/s11705-008-0056-6

RESEARCH ARTICLE

Effect of textural property of coconut shell-based activated carbon on desorption activation energy of benzothiophene

Moxin YU, Zhong LI (✉), Hongxia XI, Qibin XIA, Shuwen WANG

College of Chemical and Energy Engineering, South China University of Technology, The Key Laboratory of Enhanced Heat Transfer and Energy Conversation, Ministry of Education, Guangzhou 510640, China

Abstract In this work, the effect of the textural property of activated carbons on desorption activation energy and adsorption capacity for benzothiophene (BT) was investigated. BET surface areas and the textural parameters of three kinds of the activated carbons, namely SY-6, SY-13 and SY-19, were measured with an ASAP 2010 instrument. The desorption activation energies of BT on the activated carbons were determined by temperature-programmed desorption (TPD). Static adsorption experiments were carried out to determine the isotherms of BT on the activated carbons. The influence of the textural property of the activated carbons on desorption activation energy and the adsorption capacity for BT was discussed. Results showed that the BET surface areas of the activated carbons, SY-6, SY-13 and SY-19 were 1106, 1070 and 689 $m^2 \cdot g^{-1}$, respectively, and their average pore diameters were 1.96, 2.58 and 2.16 nm, respectively. The TPD results indicated that the desorption activation energy of BT on the activated carbons, SY-6, SY-19 and SY-13 were 58.84, 53.02 and 42.57 KJ/mol, respectively. The isotherms showed that the amount of BT adsorbed on the activated carbons followed the order of SY-6 > SY-19 > SY-13. The smaller the average pore diameter of the activated carbon, the stronger its adsorption for BT and the higher the activation energy required for BT desorption on its surface. The Freundlich adsorption isotherm model can be properly used to formulate the adsorption behavior of BT on the activated carbons.

Keywords activated carbon, benzothiophene, desorption activation energy, average pore diameter, adsorption equilibrium

Translated from *Journal of Functional Materials*, 2007, 38(10): 1664–1668 [译自: 功能材料]

E-mail: cezhli@scut.edu.cn

1 Introduction

Deep desulfurization of transportation fuels has received much attention in the research community worldwide due to increasingly stringent regulations and fuel specifications in many countries since combustion of the fuels containing sulfur produces SO_2. The US EPA mandates a reduction in gasoline and diesel sulfur levels from the current levels of 300–500 ppmw to 30 ppmw and 15 ppmw, respectively to be implemented by 2006. In 2010, the maximum S-content will be limited to 10 ppmw. European legislation also restricts the sulfur level to less than 50 ppmw for both fuels by 2005 and 10 ppmw by 2008 [1]. For environmental protection and market competition, the Chinese government sets the objectives for the sulfur level to less than 10 ppmw by 2010 from the current levels of less than 800 ppmw for gasoline and 2000 ppmw for diesel except in several big cities like Beijing and Shanghai where it mandates 150 ppmw. Hence, considerable effort is being made to remove the organosulfur molecules from the fuel to obtain sulfur-free or ultra-low-sulfur fuel.

The major sulfur compounds that exist in current commercial diesel are the alkyl dibenzothiophenes (DBTs) with one or two alkyl groups at 4- and/or 6- position. They are considered refractory sulfur compounds because of the steric hindrance of the alkyl groups in traditional hydrodesulfurization (HDS) [1]. Consequently, it is difficult or very costly to use existing HDS technology to reduce the sulfur in diesel fuel to less than 10 ppmw [1]. So, alternative technologies are of particular interest to obtain sulfur-free fuels. One new approach for desulfurization is by selective adsorption of thiophenes on adsorbents. This method might be the most economical way for the removal of thiophenes. It is well known that the adsorbent is the core of adsorption technology. In recent years, a number of desulfurization adsorbents have been studied. Song et al. of the Pennsylvania State University explored a process of selective adsorption for removing

sulfur (PSU-SARS) over various materials under ambient conditions for fuel cell and refinery applications [2–4]. Various adsorbents including metals, metal halides, metal oxides, metal sulfides and modified zeolites are being synthesized and evaluated [5–7]. Among several types of adsorbents explored, Ni-based adsorbents exhibited better performance for removing sulfur compounds [7]. Yang and coworkers have developed a variety of π-complexation-based sorbents obtained by ion exchanging zeolites with different metal cations. Among them, the Cu(I)/Y-zeolite had the best adsorption performance for thiophenic sulfur [8–11]. The activated carbons with large surface areas, rich pore structures and abundant surface groups were also used in desulfurization. Activated carbon, zeolite 5A and zeolite 13X were used for Naphtha desulfurization [12,13]. Zeolite 13X showed some capacity for sulfur at low concentration. At higher concentration, the capacity of activated carbon was three times greater than that of 13X zeolite. Zeolite 5A was unfavorable for sulfur sorption from naphtha. More recently, Kim et al. found that activated carbon showed higher adsorptive capacity and selectivity for sulfur compounds in desulfurization of a model diesel [14] especially for the sulfur compounds with methyl substituents such as 4,6-methyldibenzothiophene. Also, Hernandez-Maldonado et al. reported that using activated carbon as adsorbent in a guard bed can improve the adsorptive performance of Cu(I)-Y zeolites [15]. The activated carbon has been proven to adsorb sulfur compounds. However, it cannot be industrially used because of its low desulfurization capacity. In addition, the adsorption mechanism of organic sulfur on activated carbon is not clear. Therefore, a study of the effect of surface and textural property of activated carbon on its adsorption of sulfur would be very useful.

The purpose of this work is to investigate the effects of porosity of the activated carbon on the activation energy for benzothiophene (BT) desorption from the surface of the activated carbons by means of TPD (temperature-programmed desorption technique) and its adsorption capacity for BT.

2 TPD model and theory

TPD is a technique of surface analysis [16–19] usually employed to estimate binding energy between an adsorbate and an adsorbent and activation energy of desorption, which can be used to value the adsorbents. Basically, some kind of adsorbate is adsorbed onto the adsorbent, and then the adsorbent is heated with flowing inert gas in such a controlled way that the adsorbent temperature varies linearly with time. As the temperature becomes high enough, the adsorbate will be desorbed gradually. In a TPD experiment, a GC or a mass spectrometer is used to measure the rate of adsorbate desorption from the adsorbent. Using TPD, one can know how strongly molecules are bound to the surface of the adsorbent. The TPD spectrum is a plot of the desorption rate of the adsorbate as a function of the sample temperature [17–20].

Assume that the kinetics of the desorption process follow first order kinetics

$$\frac{r_{\mathrm{d}}}{N_{\mathrm{s}}} = -\frac{\mathrm{d}\theta_{\mathrm{A}}}{\mathrm{d}t} = k_{\mathrm{d}}\theta_{\mathrm{A}}, \tag{1}$$

where r_{d} (mol/min) is desorption rate of a component A from unit adsorbent, N_s (mol/cm^2) is the maximum concentration of the component A on unit surface of the adsorbent, θ_{A} is the transient coverage of the component A and t is time (min). Furthermore, k_{d} is defined as follows

$$k_{\mathrm{d}} = k_0 \exp\left(-\frac{E_{\mathrm{d}}}{\mathrm{R}T}\right), \tag{2}$$

where k_0 is coefficient of desorption rate, E_{d} is activation energy of desorption (kJ/mol), and R is gas constant. Substituting Eq. (2) into Eq. (1), one can get

$$\frac{r_{\mathrm{d}}}{N_{\mathrm{s}}} = -\frac{\mathrm{d}\theta_{\mathrm{A}}}{\mathrm{d}t} = k_0\theta_{\mathrm{A}} \exp\left(-\frac{E_{\mathrm{d}}}{\mathrm{R}T}\right). \tag{3}$$

Suppose that in the TPD experiment the temperature, T (K), varies with time.

$$T = T_0 + \beta_{\mathrm{H}} t, \tag{4}$$

where β_{H} is the heating rate, K/min. When the adsorbent is heated, the adsorbate begins to be desorbed. If inert gas such as argon is used to purge the adsorbent packed in the differential fixed bed, the dependence of the desorption rate of adsorbate on time or temperature, which is also called the TPD curve, can be obtained by means of on-line gas chromatography. With increasing temperature, the desorption rate increases gradually and then attains the maximum at which the peak of the TPD curve corresponds to the temperature T_{p}. After that, the desorption rate decreases gradually. The time derivative of Eq. (3), can be expressed as

$$\begin{aligned}\frac{1}{N_{\mathrm{s}}}\frac{\mathrm{d}r_{\mathrm{d}}}{\mathrm{d}t} = {} & k_0\left(\frac{\mathrm{d}\theta}{\mathrm{d}t}\right)\exp\left(-\frac{E_{\mathrm{d}}}{\mathrm{R}T}\right) \\ & + k_0\theta_{\mathrm{p}}\left(\frac{E_{\mathrm{d}}}{\mathrm{R}}\right)\frac{1}{T^2}\exp\left(-\frac{E_{\mathrm{d}}}{\mathrm{R}T}\right)\left(\frac{\mathrm{d}T}{\mathrm{d}t}\right).\end{aligned} \tag{5}$$

As seen generally in the curve of TPD, the maximum in the desorption rate will occur at $\mathrm{d}r_{\mathrm{d}}/\mathrm{d}t = 0$. Therefore, by letting $\mathrm{d}r_{\mathrm{d}}/\mathrm{d}t = 0$, the peak temperature T_{p} corresponding to the peak of the TPD curve can be mathematically determined. This can be also measured experimentally. Substituting $T = T_{\mathrm{p}}$ into Eq. (5), one can get

$$\frac{1}{N_s}\frac{dr_d}{dt}=k_0\left(\frac{d\theta}{dt}\right)\exp\left(-\frac{E_d}{RT_p}\right)+k_0\theta_p\left(\frac{E_d}{R}\right)\frac{1}{T_p^2}\exp\left(-\frac{E_d}{RT_p}\right)\left(\frac{dT}{dt}\right)=0. \quad (6)$$

Substituting Eqs. (3) and (4) into Eq. (6) and then canceling like terms, one can get

$$k_0\exp\left(-\frac{E_d}{RT_p}\right)=\frac{\beta_H E_d}{RT_p^2}. \quad (7)$$

Rearranging Eq. (7) yields

$$\ln\left(\frac{RT_p^2}{\beta_H}\right)=\frac{E_d}{R}\left(\frac{1}{T_p}\right)+\ln\left(\frac{E_d}{k_0}\right). \quad (8)$$

If a series of TPD experiments are conducted at different heating rates, corresponding TPD curves and values T_p could be obtained. After that, a plot of $\ln(RT_P^2/\beta_H)$ versus $1/T_p$ will yield a line with slope E_d/R, from which E_d can be determined. k_0 can be also obtained from the intercept of the line.

3 Experimental

3.1 Materials and instruments

The adsorbate, benzothiophene (98%), was purchased from Acros Organics, New Jersey, USA. The activated carbons, namely SY-6, SY-13, SY-19 (40–60 mesh), based on coconut shell was supplied by the Zhaoyang Senyuan Activated Carbon Company, China. The model diesel fuel (MDF) used in this work is a mixture of *n*-octane and BT (10 mmol-S/L).

The TPD process was performed in a fixed-bed mini reaction furnace (LW4, Jiangsu, China). The diameter of the differential fixed bed was 0.2 cm and its length was 0.5 cm. Desorption temperature was controlled by a temperature-programmed controller (Al-708, Xiamen, China). The desorbed products were continuously determined by a gas chromatograph with a flame ionization detector (GC-950, Shanghai, China).

3.2 TPD experiments

Figure 1 shows the flow chart of the TPD equipment. The TPD experiments were conducted at different heating rates from 5 to 10 K/min. The TPD samples were prepared by impregnating the three activated carbons with 5 mL of 0.02 M solution of BT in methanol for 30 min. Subsequently the samples were filtered and kept at room temperature for 24 h under a continuous flow of air to remove the residual methanol. In each experiment, the sample that had adsorbed BT was packed in a stainless steel reaction tube whose inner diameter and length were 0.2 and 0.5 cm, respectively. Subsequently, the stainless steel tube was placed in a reaction furnace and then heated in high-purity N_2 which was flowing at a constant rate 50 mL/min. The desorbed BT was measured by GC at the outlet of the column and effluent curves, called TPD curves were recorded.

3.3 Adsorption isotherm measurements [20]

The equilibrium adsorption isotherms for BT from *n*-octane solution on SY-6, SY-13 and SY-19 were determined separately at 30°C and 50°C using the bottle-point method. Different amounts of activated carbons were weighed and placed in bottles with 5 mL of MDF (10 mmol-S/L). The bottles were then capped and placed on a shaker for 24 h. Subsequently, the equilibrium concentration of BT solution (C_i*) was determined using an Agilent liquid chromatograph with UV-Visible detector. The mobile phase was methanol (HPLC-grade). The

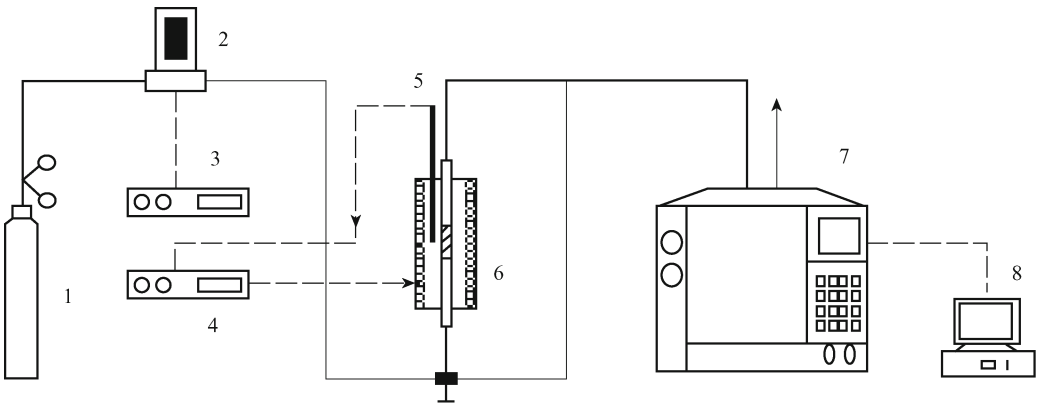

1 N_2; 2 Mass flow meter; 3 Mass flow rate controller; 4 Temperature controller; 5 Thermal couple; 6 Mini reaction furnace; 7 GC (FID); 8 GC work station

Fig. 1 Schematic flow diagram of Temperature Programmed Desorption (TPD)

analyses were performed at 298 K at a flow rate of 1.0 mL/min. The wavelength of the UV detector was set to 220 nm. Then the equilibrium adsorption capacity q_i was calculated from a material balance equation:

$$q_i = \frac{V}{M_i} \times \left(C_0 - C_i^*\right), \tag{9}$$

where q_i is amount adsorbed in equilibrium with the concentration of BT in fluid phase (mmol-S/kg), C_0 is the initial concentration of BT in fluid phase (mmol-S/L), C_i* is the equilibrium concentration of BT in the fluid phase (mmol-S/L), V is the volume of solution (L) and M_i is the weight of the activated carbon used (kg).

4 Results and discussion

4.1 Textural properties

Nitrogen adsorption experiments were carried out at 77 K using an accelerated surface area and porosimeter system (ASAP 2010, Micromeritics) to determine the textural properties of all the activated carbons studied. Figure 2 shows the nitrogen adsorption isotherms for the activated carbons SY-6, SY-13 and SY-19. It indicates that the SY-6 had mainly micropores and mesopores, SY-13 had large pores, mesopores and micropores and SY-19 had mainly micropores. Table 1 lists the structure parameters of the different activated carbons.

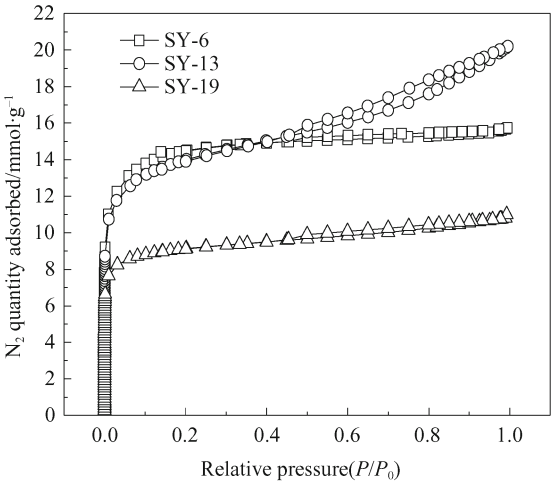

Fig. 2 N_2 adsorption-desorption isotherm of activated carbons

4.2 Activation energy for desorption of BT on various activated carbons

Figure 3 shows TPD curves of the three different activated carbons, SY-6, SY-13 and SY-19 at a heating rate of 5 K/min. There were no obvious peaks in the TPD curves obtained as none of the activated carbons was associated with any adsorbate.

Figures 4–6 show TPD curves of BT desorption on three different activated carbons which adsorbed BT at different heating rates from 5 to 10 K/min. There were two peaks in the TPD curves. Each peak represented a

Table 1 Porous structure parameters of different activated carbons

Activated carbon	BET Surface area/ $m^2 \cdot g^{-1}$	Micropore Surface area/$m^2 \cdot g^{-1}$	Average pore diameter/ nm	Mesopore volume/$cm^3 \cdot g^{-1}$	Total pore volume/$cm^3 \cdot g^{-1}$
SY-6	1106	756	1.96	0.349	0.542
SY-13	1070	665	2.58	0.308	0.692
SY-19	689	532	2.16	0.228	0.373

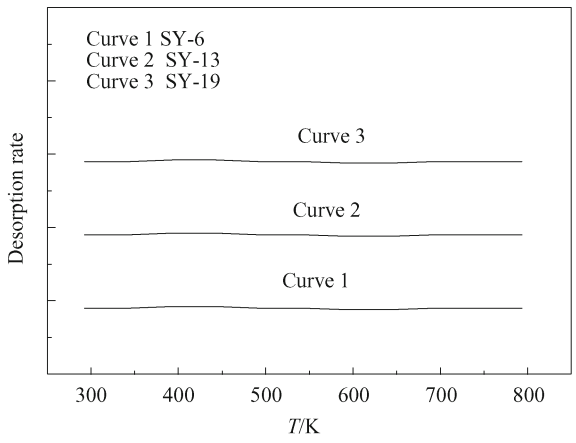

Fig. 3 TPD curves of three different activated carbons, experimental condition: β_H = 5 K/min, flowrate: 50 mL/min

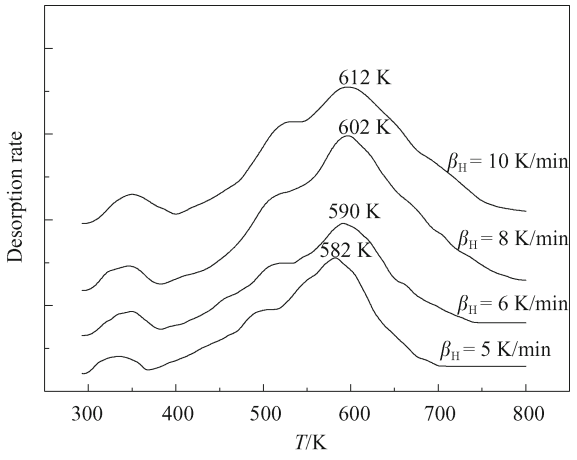

Fig. 4 Effect of β_H on TPD curves for desorption of BT SY-6 AC (flowrate: 50 mL/min)

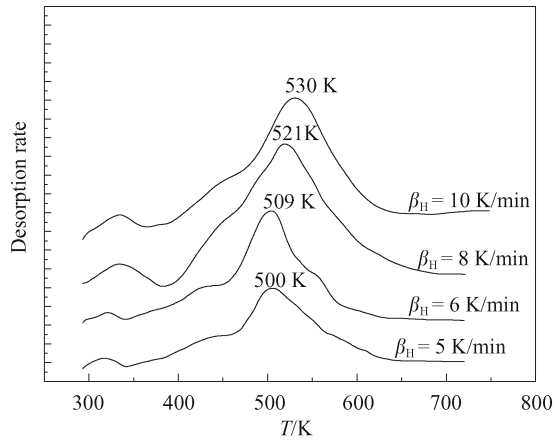

Fig. 5 Effect of β_H on TPD curves for desorption of BT on SY-13 AC (flowrate: 50 mL/min)

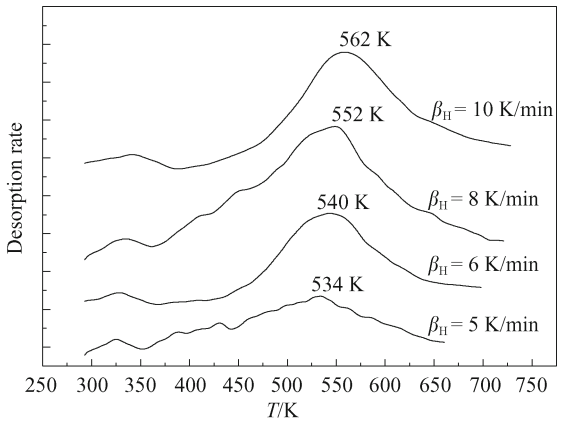

Fig. 6 Effect of β_H on TPD curves for desorption of BT on SY-19 AC (flowrate: 50 mL/min)

different kinetic process: the first one was the desorption peak of residual solvent and the second one was that of BT adsorbed on the activated carbon. The peak temperature increased with an increase in heating rate. Once a series of TPD curves of BT desorption on the activated carbon at different heating rates were available, the desorption activation energy of BT can be estimated using Eq. (8). The linear dependence on $1/T_P$ of $\ln(RT_P^2/\beta_H)$ for the TPD of BT on the activated carbons were shown in Fig. 7. From the slope of these lines, activation energy E_d can be calculated. The calculation values of the desorption activation energy of BT on the activated carbons are listed in Table 2.

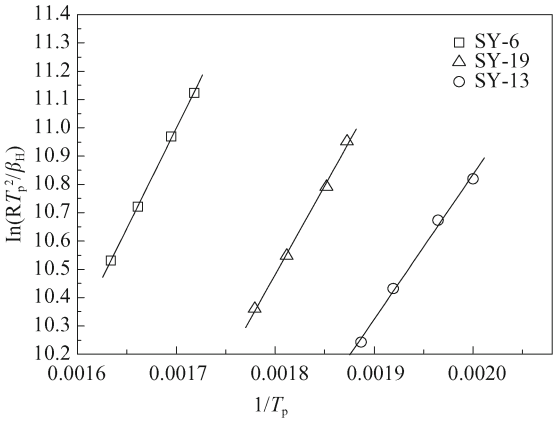

Fig. 7 Linear dependence between $\ln(RT_P/\beta_H)$ and $1/T_P$ for TPD of BT on activated carbons

It can be seen from Table 2 that the activation energy of BT desorption on the activated carbons SY-6, SY-19 and SY-13 were 58.84 KJ/mol, 53.02 KJ/mol and 42.57 KJ/mol, respectively. The activation energy for the desorption of BT on the activated carbons followed the order: SY-6 > SY-19 > SY-13. Generally, the higher the desorption activation energy, the more difficult the desorption of the adsorbate from an adsorbent. In other words, the higher the desorption activation energy, the stronger the adsorption of the adsorbate on the surfaces of the adsorbent. The interaction between BT and SY-6 was the strongest and the interaction between BT and SY-13 was the weakest. It can be seen from Table 1 that the average pore diameter of activated carbon followed the order: SY-6 > SY-19 > SY-13. The larger the average pore diameter of activated carbon, the smaller its adsorption for BT and the smaller the average pore diameter of activated carbon, the larger its adsorption for BT. It is evident that the pore structure of activated carbon plays an important role in its adsorption of the adsorbate.

4.3 Adsorption isotherms of BT on various activated carbons

Figures 8 and 9 showed the adsorption isotherms of BT on different activated carbons at 30°C and 50°C, respectively. It can be seen from the figures that the adsorption capacity of BT on the activated carbons followed the order: SY-6 > SY-19 > SY-13. It was also found that the adsorption capacity of BT on different activated carbons decreased with increase in temperature.

Table 2 Activation energy of desorption of BT on different activated carbons

Activated carbon	T_p (K) corresponding to peak of TPD curves at different heating rate β_H/K·min^{-1}				E_d/kJ·mol^{-1}
	5	6	8	10	
SY-6	582	590	602	612	58.84
SY-19	534	540	552	562	53.02
SY-13	500	509	521	530	42.57

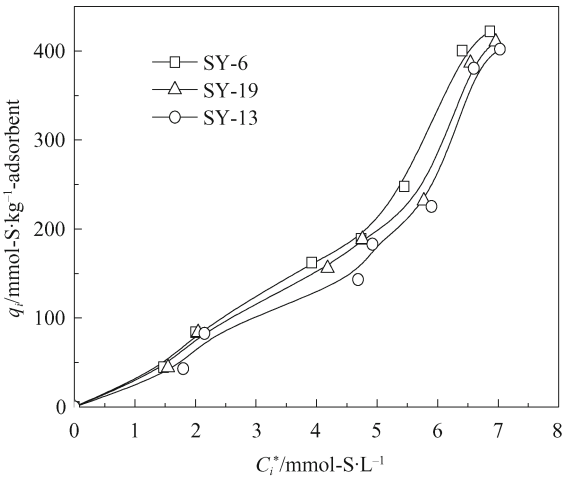

Fig. 8 Adsorption isotherm of BT on different activated carbons at 30°C

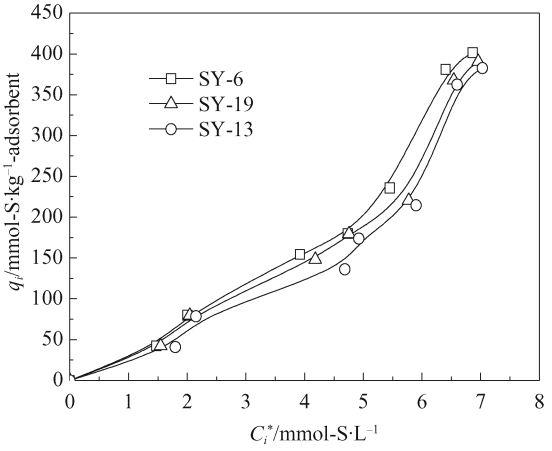

Fig. 9 Adsorption isotherm of BT on different activated carbons at 50°C

4.4 Langmuir and Freundlich adsorption isotherms

Different mathematical models have been proposed to represent liquid adsorption processes under certain conditions. Among them, the Langmuir and Freundlich adsorption isotherms are two models often used to describe the experimental data. Langmuir derived the simple equation for the equilibrium adsorption isotherm as

$$q_i = \frac{q_{\max} \mathrm{b} C_i^*}{1 + \mathrm{b} C_i^*}. \tag{10}$$

Freundlich isotherms are empirical but useful in industrial practice. This isotherm can be written as

$$q_i = K_\mathrm{f} C_i^* n, \tag{11}$$

where q_i is the amount adsorbed in equilibrium with the concentration of solute in fluid phase (mmol-S/kg), $q_{\max}$ is the maximum adsorption amount (mmol-S/kg), C_i* is the equilibrium concentration of solute in fluid phase (mmol-S/L)and b is the equilibrium constant of adsorption. In Eq. (11), K_f and n are Freundlich equilibrium constants of adsorption.

The Langmuir and Freundlich adsorption isotherms were used to fit the experimental data in Figs. 8 and 9, respectively. The results are separately listed in Tables 3 and 4. It can be seen from Tables 3 and 4 that the correlation coefficients (r^2) obtained by the Freundlich adsorption isotherm were better than that by the Langmuir adsorption isotherms. So the Freundlich model can be properly used to formulate the adsorption behavior of BT on the activated carbons.

Table 3 Parameters obtained by fitting of Langmuir isotherm

Activated carbon	Temperature/°C	Langmuir		
		$q_{\max}$/mmol·kg^{-1}	B	r^2
SY-6	30	1195.63	0.081	0.6004
	50	1004.69	0.074	0.6901
SY-13	30	1053.75	0.079	0.6401
	50	978.13	0.069	0.6183
SY-19	30	1102.82	0.082	0.6743
	50	985.75	0.078	0.6059

Table 4 Parameters obtained by fitting of Freundlich isotherm

Activated carbon	Temperature/°C	Freundlich		
		K_f	N	r^2
SY-6	30	27.68	1.356	0.9847
	50	26.04	1.283	0.9855
SY-13	30	21.05	1.422	0.9734
	50	19.85	1.356	0.9821
SY-19	30	26.31	1.341	0.9793
	50	25.03	1.284	0.9736

4.5 Effect of surface area and pore structure of activated carbon on its adsorption for BT

It can be seen from Table 1 that both the BET surface areas and the micropore areas of the activated carbons followed the order: SY-6 > SY-13 > SY-19. However, the adsorption capacity of BT on the activated carbons obtained by experimental data followed the order: SY-6 > SY-19 > SY-13. Though the surface area of SY-13 is larger than that of SY-19, the adsorption capacity of SY-13 is smaller than that of SY-19. This is probably due to the large pore diameter of SY-13. From Fig. 2 and Table 1, the average pore diameter of SY-13 is the largest among three activated carbons because it had a great number of large pores and mesopores. The average pore diameters followed the order SY-13 > SY-19 > SY-6, which is different from the order of the adsorption capacity of BT on the activated carbons. Furthermore, it can be found from Table 2 that the smaller the average pore diameter of the activated carbon, the

larger the activation energy of BT desorption. The results showed that the smaller the average pore diameter of the activated carbon, the stronger its adsorption for BT and thus, the larger the adsorption capacity for BT. So it can be concluded that the average pore diameter of activated carbon plays a more important role than its surface area and pore volume in adsorption for BT in this work.

5 Conclusions

The pore structure of activated carbon plays an important role in desorption activation energy and its adsorption capacity for BT. The BET surface areas of the activated carbons, SY-6, SY-13 and SY-19 were 1106, 1070 and 689 $m^2 \cdot g^{-1}$, respectively, and their average pore diameters were 1.96, 2.58 and 2.16 nm, respectively. The TPD results indicated that the desorption activation energy of BT on the activated carbons, SY-6, SY-19 and SY-13 were 58.84, 53.02 and 42.57 KJ/mol, respectively. The isotherms showed that the amount of BT adsorbed on the activated carbons followed the order SY-6 > SY-19 > SY-13. The smaller the average pore diameter of the activated carbon, the stronger its adsorption for BT and the higher the activation energy required for BT desorption on its surface. The Freundlich adsorption isotherm model can be properly used to formulate the adsorption behavior of BT on the activated carbons.

Acknowledgements The authors are very grateful to thank the National Natural Science Foundation of China (Grant No. 20336020) for financial support.

References

1. Song C. An overview of new approaches to deep desulfurization for ultra-clean gasoline, diesel fuel and jet fuel. Catal Today, 2003, 86: 211–263
2. Song C, Ma X. New design approaches to ultra-clean diesel fuels by deep desulfurization and deep dearomatization. Appl Catal B: Environ, 2003, 41: 207–238
3. Ma X, Sun L, Song C. A new approach to deep desulfurization of gasoline, diesel fuel and jet fuel by selective adsorption for ultra-clean fuels and for fuel cell applications. Catal Today, 2002, 77: 107–116
4. Ma X, Velu S, Kim J H, Song C. Deep desulfurization of gasoline by selective adsorption over solid adsorbents and impact of analytical methods on ppm-level sulfur quantification for fuel cell applications. Appl Catal B: Environ, 2005, 56: 137–147
5. Velu S, Ma X, Song C. Selective adsorption for removing sulfur from jet fuel over zeolite-based adsorbents. Ind Eng Chem Res, 2003, 42: 5293–5304
6. Song C. Fuel processing for low-temperature and high-temperature fuel cells: challenges and opportunities for sustainable development in the 21st entury. Catal Today, 2002, 77: 17–49
7. Velu S, Ma X, Song C, Namazian M, Sethuraman S, Venkataraman G. Desulfuriation of JP-8 Jet fuel by selective adsorption over a Ni-based adsorbent for micro solid oxide fuel cells. Energy Fuels, 2005, 19: 1116–1125
8. Yang R T, Hernandez-Maldonado A J, Yang F H. Desulfurization of transportation fuels with zeolites under ambient conditions. Science, 2003, 301: 79–81
9. Hernandez-Maldonado A J, Yang F H, Qi G S, Yang R T. Desulfurization of transportation fuels by π-complexation sorbents: Cu(I)-, Ni(II)-, and Zn(II)-zeolites. Appl Catal B: Environ, 2005, 56: 111–126
10. Takahashi A, Yang F H, Yang R T. New sorbents for desulfurization by π-complexation: thiophene/benzene adsorption. Ind Eng Chem Res, 2002, 41: 2487–2496
11. Hernandez-Maldonado A J, Stamatis S D, Yang R T, He A Z, Cannella W. New sorbents for desulfurization of diesel fuels via π-complexation: layered beds and regeneration. Ind Eng Chem Res, 2004, 43: 769–776
12. Salem S H A B. Naphtha desulfurization by adsorption. Ind Eng Chem Res, 1994, 33: 336–340
13. Salem S H A B, Hamid H S. Removal of sulfur compounds from naphtha solutions using solid adsorbents. Chem Eng Technol, 1997, 20: 342–347
14. Kim J H, Ma X, Zhou A, Song C. Ultra-deep desulfurization and denitrogenation of diesel fuel by selective adsorption over three different adsorbents: a study on adsorptive selectivity and mechanism. Catal Today, 2006, 111: 74–83
15. Hernandez-Maldonado A J, Yang R T. Desulfurization of commercial liquid fuels by selective adsorption via π-Complexation with Cu(I)-Y Zeolite. Ind Eng Chem Res, 2003, 42: 3103–3110
16. Xi H X, Li Z, Zhang H B, Li X, Hu X J. Estimation of activation energy for desorption of low-volatility dioxins on zeolites by TPD technique. Sep Purif Technol, 2003, 31: 41–45
17. Li Z, Wang H J, Xi H X, Xu K F, Wen J. Estimation of activationenergy of desorption of *n*-hexane on activated carbons by TPD technique. Chinese Journal of Reactive Polymers, 2001, 10: 113–120 (in Chinese)
18. Richard I M. Wiley Series in Chemical Engineering. First Edition. New York: Wiley-Interscience Publication, 1996, 482–580.
19. Xia Q B, Li Z, Xi H X, Xu K F. Activation energy for dibenzofuran desorption from Fe^{3+}/TiO_2 and Ce^{3+}/TiO_2 photocatalysts coated onto glass fibers. Adsorpt Sci Technol, 2005, 23: 357–366
20. Li Z, Wang H J, Xi H X, Xia Q B, Han J L, Luo L A. Estimation of activation energy of desorption of *n*-Hexanol from activated carbons by the TPD technique. Adsorpt Sci Technol, 2003, 21: 125–133